

Real-Time Study of CVD Growth of Silicon Oxide on Rutile $\text{TiO}_2(110)$ Using Tetraethyl Orthosilicate

Shilpi Chaudhary,[†] Ashley R. Head,[†] Rocío Sánchez-de-Armas,[‡] Héloïse Tissot,^{§,||} Giorgia Olivieri,^{||} Fabrice Bournel,[‡] Lars Montelius,[†] Lei Ye,[#] François Rochet,^{§,||} Jean-Jacques Gallet,^{§,||} Barbara Brenna,[‡] and Joachim Schnadt^{*†}

[†]Division of Synchrotron Radiation Research, Department of Physics, Lund University, Box 118, 221 00 Lund, Sweden

[‡]Materials Theory, Department of Physics and Astronomy, Uppsala University, Box 516, 751 20 Uppsala, Sweden

[§]Sorbonne Universités, UPMC Univ Paris 06, UMR 7614, Laboratoire de Chimie Physique - Matière et Rayonnement, 11 rue Pierre et Marie Curie, 75231 Paris Cedex 05, France

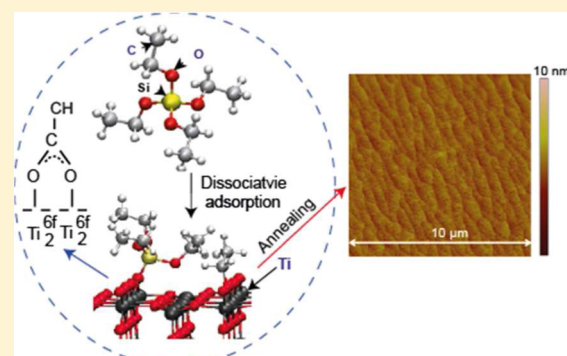
^{||}Synchrotron SOLEIL, L'Orme des Merisiers, 91190 Saint Aubin, France

[#]Division of Solid State Physics, Department of Physics, Lund University, Box 118, 221 00 Lund, Sweden

^{*}Division of Pure and Applied Biochemistry, Lund University, Box 124, 221 00 Lund, Sweden

Supporting Information

ABSTRACT: The interaction of the rutile $\text{TiO}_2(110)$ surface with tetraethyl orthosilicate (TEOS) in the pressure range from UHV to 1 mbar as well as the TEOS-based chemical vapor deposition of SiO_2 on the $\text{TiO}_2(110)$ surface were monitored in real time using near-ambient pressure X-ray photoelectron spectroscopy. The experimental data and density functional theory calculations confirm the dissociative adsorption of TEOS on the surface already at room temperature. At elevated pressure, the ethoxy species formed in the adsorption process undergoes further surface reactions toward a carboxyl species not observed in the absence of a TEOS gas phase reservoir. Annealing of the adsorption layer leads to the formation of SiO_2 , and an intermediate oxygen species assigned to a mixed titanium/silicon oxide is identified. Atomic force microscopy confirms the morphological changes after silicon oxide formation.



I. INTRODUCTION

Chemical vapor deposition (CVD) and the closely related technique of atomic layer deposition (ALD) are among the most important methods to achieve controlled growth of thin films, in particular, within the semiconductor technology domain.¹ The choice of CVD/ALD parameters has an important impact on the properties of the grown film and influences the film structure, roughness, and optical properties.² Since the atomic-scale surface chemistry during growth is of essential importance for the development of these properties, it is fundamental that a true understanding of the surface chemical processes is obtained which goes beyond idealized models.² Surface science microscopy and spectroscopy methods, including laboratory- and synchrotron-based electron spectroscopy, can contribute with highly detailed information on surface structure and processes of relevance to CVD and ALD, and, indeed, ex situ (post mortem) surface science characterization has been and is playing an important role in the formulation of growth models (for a few examples, see, e.g., refs 3–7). While such post mortem investigations are very helpful in the determination of the properties of the already

grown thin films, they can deliver neither a true identification of species during growth nor an elucidation of the growth kinetics. Moreover, the role of the nature of the support and of potential defects can be assessed to only a limited extent. In situ methods in general and near-ambient pressure X-ray photoelectron spectroscopy (NAPXPS) in particular have the ability for real-time monitoring of the surface chemistry during the growth and can address the shortcomings of post mortem measurements.^{8–10} Therefore, these techniques can provide deeper insight into the role of the chosen CVD/ALD parameters, dynamic surface structure, and defects (please note that the term in situ is here used in the surface science rather than CVD/ALD sense: it denotes measurement at reaction conditions rather than measurement in vacuum after performing the CVD/ALD reaction in a reactor directly connected to the characterization chamber).

Received: May 25, 2015

Revised: July 23, 2015

Published: July 24, 2015

Here, we use X-ray photoelectron spectroscopy (XPS), NAPXPS, and density functional theory (DFT) to investigate the interaction of tetraethyl orthosilicate (TEOS), an organosilane, with the rutile $\text{TiO}_2(110)$ surface. The studied pressure regime extends from typical ultrahigh vacuum (UHV) pressures in the 10^{-9} up to the mbar range of practical importance to real ALD and CVD processes, and the investigated temperatures lie in between room temperature and a CVD-relevant maximum temperature of 810 K. Since the 1960s TEOS has been used as a precursor in the growth of silicon oxide thin films,^{11,12} and the TEOS-based CVD process has practical importance in the micro- and nanoelectronics industry.¹³ In the present paper, we target the $\text{SiO}_2/\text{TiO}_2$ interface, a material combination which, e.g., has been suggested to be of interest for intermediate refractive index,¹⁴ superhydrophilic,¹⁵ and photocatalytic¹⁶ materials. The interaction of limited doses of TEOS with a clean $\text{TiO}_2(110)$ surface as well as one onto which water had been predosed has been studied previously in UHV to a very detailed level by Gamble et al.¹⁷ They found that a disordered SiO_2 overlayer is formed upon annealing as the result of dissociative adsorption of TEOS. We draw on this previous study here and find similarities as well as differences in the surface chemistry in UHV and at elevated pressure.

II. EXPERIMENTAL AND THEORETICAL METHODS

The experiments were performed at the NAPXPS end station of the TEMPO beamline at the SOLEIL synchrotron facility in France.¹⁸ The end station consists of a preparation chamber and an analysis chamber with base pressures of 1×10^{-9} mbar and 5×10^{-9} mbar, respectively, at the time of the experiment. In addition, the instrument has further chambers for sample transfer and ex situ preparation. The preparation chamber is equipped with a sputter gun and LEED optics employed for surface preparation and basic characterization. The analysis chamber is equipped with a near-ambient pressure SPECS Phoibos 150-NAP electron analyzer, protected from high pressures in the main chamber by a set of differential pumping stages. The nozzle that separates the sample volume of the analysis chamber from the first differential pumping stage of the analyzer has a diameter of 0.3 mm; the working distance between nozzle and sample is around twice the diameter so the path of the photoelectrons through the vapor is minimized and hence the transmission maximized.⁸ Thus, samples can be measured in pressures between UHV and around 25 mbar. The detector is a 3D: x , y , t delay line detector. A windowless beamline entrance with three differential pumping stages separates the analysis chamber from the beamline, keeping the pressure at the last optical element in the low 10^{-9} mbar regime.

The rutile $\text{TiO}_2(110)$ single crystal of dimensions $10 \times 10 \times 1$ mm³ was purchased from PI-Kem, England. The crystal was mounted with molybdenum screws and clamps on a sample holder attached with a borolectric heater. The K-type thermocouple was attached with a clamp on the top of crystal. The crystal was cleaned by several cycles of argon ion sputtering for 10 min at an energy of 1 keV, followed by annealing at 600 °C for 10 min. A sharp (1×1) low-energy electron diffraction (LEED) pattern was observed from the clean crystal (inset in Figure 1). Using XPS it was found that the TiO_2 crystal was somewhat more heavily reduced than reported in previous studies in spite of the fact that the same standard cleaning procedure was applied.¹⁹ The stronger reduction is seen from the low-binding energy shoulder of

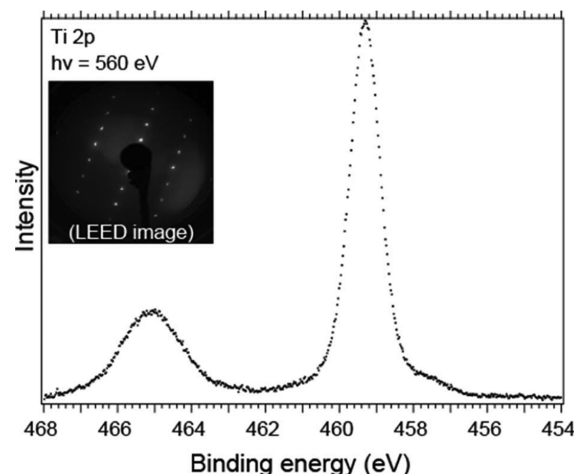


Figure 1. Ti 2p XP spectra obtained on the clean surface. The peak at 465 eV binding energy is the $\text{Ti} 2\text{p}_{1/2}$ line, and that at 495.5 eV is the $\text{Ti} 2\text{p}_{3/2}$ line. The low-binding-energy shoulder of the latter reflects the presence of Ti^{3+} defects. The inset shows LEED image taken after the last cleaning cycle exhibiting a perfect (1×1) pattern.

the Ti 2p_{3/2} peak in the spectrum in Figure 1 attributed to Ti^{3+} point defects. It seems to be an artifact of the crystal growth. From the spectral intensities of the Ti^{4+} and Ti^{3+} components of the Ti 2p_{3/2} peak we derive an upper limit of 14.3% for the bridging oxygen concentration (see eqs S1 and S2 in the Supporting Information). In the derivation it was assumed that the entire intensity of the Ti^{3+} component is due to bridging oxygen vacancies, which certainly is an overestimation, since also subsurface and bulk defects contribute to this component.

The $\text{TiO}_2(110)$ crystal was also affected by a small K contamination. From the K 2p photoemission intensity we estimated the upper limit of this contamination to be 1 K atom per 30 surface unit cells.

TEOS was purchased from Sigma-Aldrich (purity 98%). The TEOS molecules were degassed using several freeze–pump–thaw cycles and dosed through a leak valve attached to the analysis chamber. The C 1s and Si 2p core-level spectra were recorded with photon energy of 390 eV, the O 1s spectra at 650 eV, and the Ti 2p spectra at 560 eV, with a total energy resolution of approximately 0.18, 0.23, and 0.21 eV, respectively. All spectra were calibrated using the Fermi level of a gold foil in good ohmic contact with the TiO_2 crystal. A polynomial-type background was subtracted from all spectra other than the C 1s line, for which a Shirley-type background was removed. Least square fitting of the C 1s spectra was done using Voigt line profiles. The full width at half-maximum (fwhm) of the lines was then calculated using²⁰

$$\text{FWHM} = 0.5346 \times \text{LW} + \sqrt{0.2169 \times \text{LW}^2 + \text{GW}^2}, \quad (1)$$

where LW (0.11) and GW (1.2–1.6 eV) are the Lorentzian and Gaussian FWHMs.

In order to avoid the appearance of beam damage-related features in the X-ray photoelectron (XP) spectra, the sample was moved after measurement of each of the two spectra. The moving rate was based on previous experience with TEOS.²¹ For a closely related compound, (3-aminopropyl)-triethoxysilane (APTES), with a very similar surface chemistry on $\text{TiO}_2(110)$ as that of TEOS, we have found that irradiation with soft X-rays leads to the conversion of ethoxy to carboxyl

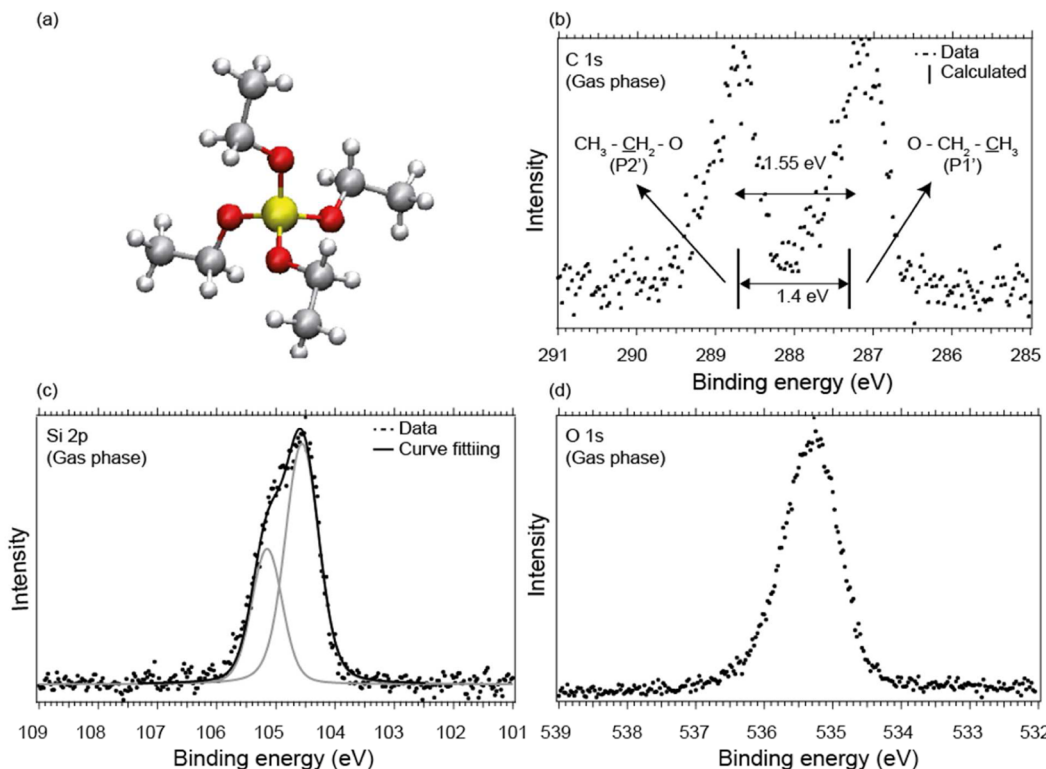


Figure 2. (a) Structure of TEOS. Medium gray spheres represent C atoms, white hydrogen, red (dark gray) oxygen, and yellow (central atom) silicon. (b) C 1s (c) Si 2p, and (d) O 1s XP spectra of the TEOS gas phase.

surface species, quite in line with irradiation by UV light.²² It is shown in the Supporting Information that for APTES under similar irradiation conditions as used here for TEOS the pristine spectra can only be observed for around 10 s, if the sample is not moved. TEOS can be expected to behave similarly, which implies that a part of the carboxylic C 1s intensity in Figure 3 probably is due to beam damage. It should be emphasized, though, that the analysis of the APTES data in the Supporting Information (Figure S1 and accompanying text) shows that a significant fraction of the conversion to a carboxyl species is intrinsic to the surface and not beam-damage-related. Due to the very similar surface chemistry of TEOS we assume the same to be true in the case presented here.

Gas-phase spectra of TEOS were recorded by moving the sample far away from the analyzer nozzle while the TEOS pressure in the chamber was at the vapor pressure limit (\sim 2 mbar). An instability in the intensity of the beam during the temperature-dependent XPS (TDXPS) measurements caused artificial structure in the spectra series in Figures 8 and 10, which is visible as sudden jumps in intensity.

The adsorption and dissociation of TEOS on the rutile TiO₂(110) surface were studied using the VASP (Vienna ab initio simulation package) code^{23–26} using the generalized gradient approximation (GGA) with the Perdew-Burke-Ernzerhof functional^{27,28} and projector-augmented wave (PAW) potentials.^{29,30} The valence electrons were described using a plane-wave basis set with a cutoff of 400 eV, and a $2 \times 2 \times 1$ Monkhorst-Pack k -points set was used.³¹ The surface was represented by a slab made of 4×2 unit cells (11.892×13.142 Å) and 4 layers (with the atoms of the 2 last layers fixed), and 22 Å of vacuum was added in the z direction to avoid the interaction between the slabs. In order to model surfaces with bridging oxygen vacancies, one bridging oxygen atom was

removed from the supercell and thus the system represents a surface with a 12.5% oxygen vacancy concentration, relatively close to experimental conditions. To study TEOS adsorption, one molecule was placed on the slab, which represents a coverage of $\theta_A = 0.125$. For the most stable structures of TEOS molecularly and dissociatively adsorbed on TiO₂, the C 1s XPS spectra were simulated using DFT as implemented in GPAW (grid-based projector-augmented wave method).^{32–34} The projector augmented wave method was used with frozen core electrons, and exchange and correlation were estimated by the Perdew–Burke–Ernzerhof (PBE) generalized gradient approximation. Periodic boundary conditions were applied and single point calculations were performed at the Γ point of the Brillouin zone. The ionization potentials (IP) of the 1 s electronic level of each carbon atom were obtained independently, as the energy difference between the ground state and the core excited state (full core), according to the Δ Kohn–Sham method.³⁵ The core–hole setup (similar to a pseudopotential) was created by using a spin-paired atomic calculation with the occupation of the core orbital decreased by one and held fixed. All theoretical IPs were shifted by 5.4 eV to lower energies in order to match the experimental spectra.

III. RESULTS

Gas Phase. For reference, gas phase spectra of TEOS (chemical structure in Figure 2a) were recorded at the room temperature vapor pressure of TEOS. The C 1s XP spectrum is shown in Figure 2b and exhibits two peaks, which we attribute to the two chemically different kinds of carbon atoms in the compound. These are denoted $\underline{\text{C}}\text{H}_3-\text{CH}_2-\text{O}-\text{Si}/\text{P}1'$ for the terminal methyl group and $\text{CH}_3-\underline{\text{CH}}_2-\text{O}-\text{Si}/\text{P}2'$ (the atoms from which photoemission occurs are underlined) for the oxygen-bonded chain carbon with separation of 1.55 eV, as

determined from a least-squares fit using asymmetric Voigt profiles with a fwhm of 1.26 eV. The intensity ratio of the $\text{CH}_3\text{---CH}_2\text{---O---Si}$ and $\text{CH}_3\text{---CH}_2\text{---O---Si}$ peaks is 1, in accordance with the stoichiometry of the molecule. The calculated XP spectrum for free TEOS molecule exhibits two peaks, one for each type of carbon ($\text{CH}_3\text{---CH}_2\text{---O---Si/P1'}$, $\text{CH}_3\text{---CH}_2\text{---O---Si/P2'}$) with a separation of ~ 1.4 eV, which is only 0.15 eV smaller than the experimental energy difference, thus validating the calculations. The theoretical value only slightly underestimates the peak separation found in the experimental spectrum. The Si 2p and O 1s gas phase spectra are shown in Figure 2c and d. Also in agreement with the chemical structure of TEOS (all four oxygen atoms are chemically equivalent), these lines exhibit a single component only. The Si 2p XP spectrum is fitted with two components representing the Si 2p_{1/2} and Si 2p_{3/2} lines with an energy difference of ~ 0.58 eV and an intensity ratio of 0.5 in agreement with the literature.³⁶

Adsorption of TEOS on $\text{TiO}_2(110)$: Low Pressure/Low Coverage Regime.

The initial adsorption of TEOS on the $\text{TiO}_2(110)$ surface at room temperature was investigated for an exposure of 4 min of TEOS at a pressure of 5×10^{-9} mbar (cf. top spectra in Figures 3 and 4 and Figure 5a). Three peaks are

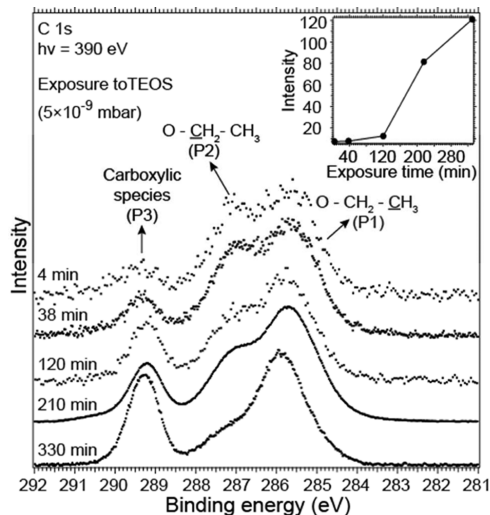


Figure 3. C 1s XP spectra for different room temperature exposures of $\text{TiO}_2(110)$ to TEOS at a pressure of 5×10^{-9} mbar. The spectra are normalized to the maximum height of the spectrum. The inset shows the increase in total C 1s intensity with exposure.

found in the C 1s spectrum: a peak at around 285.5 eV, which we label P1, a peak (P2) at around 287.0 eV, and a high binding energy peak (P3) at around 289.3 eV. As in the case of the vapor phase spectra, the two low-binding energy components are assigned to terminal methyl groups ($\text{CH}_3\text{---CH}_2\text{---O/P1}$) and oxygen-bonded ($\text{CH}_3\text{---CH}_2\text{---O/P2}$) carbon atoms, respectively. The spectral weight of these components is 1:0.75 for P1:P2. The separation between the two peaks is 1.46 eV, which is nearly the same as in the gas-phase spectrum in Figure 1 (1.55 eV). The value of the high binding energy component P3, with a spectral weight of 0.25, is in agreement with the formation of a new species. In view of the relatively high binding energy of more than 289 eV, the most likely candidate is a carboxyl species,³⁷ which is in agreement with the formation of a carboxyl requiring the reaction of a split-off ethoxy ligand with surface oxygen or hydroxyls. As outlined in

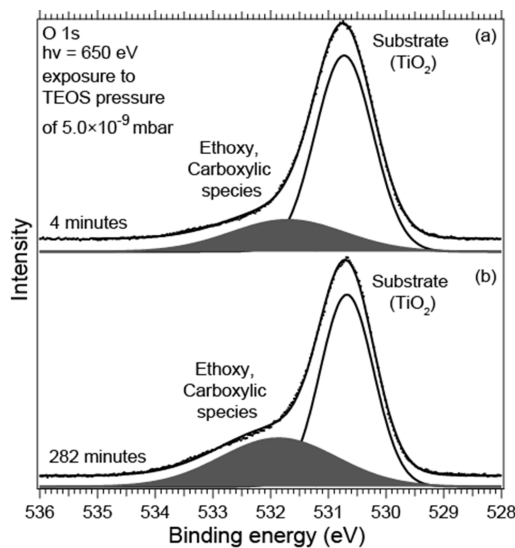


Figure 4. O 1s XP spectra taken upon exposure of the $\text{TiO}_2(110)$ surface to (a) TEOS for 4 min and to (b) 282 min at room temperature at a pressure of 5×10^{-9} mbar.

the Methods section, a fraction of the P3 intensity could be due to photoinduced conversion of ethoxy to carboxyl surface species, i.e., to beam damage. However, since care was taken to obtain spectra at fresh spots, the increase of the intensity cannot be explained by a cumulative beam damage effect, but must be related to the surface chemistry of TEOS on the $\text{TiO}_2(110)$ surface. Worth noting is that the intensity of the $\text{CH}_3\text{---CH}_2\text{---O/P1}$ peak is approximately equal to the sum of the $\text{CH}_3\text{---CH}_2\text{---O/P2}$ and carboxyl/P3 peaks. We will return to this point in the discussion.

Together with the Ti 2p XP spectra, the C 1s spectra allow estimation of the surface coverage θ_A and overlayer thickness t for the film grown from TEOS as (cf, ref 38)

$$\theta_A = \frac{\frac{I_{\text{C}1s}}{I_{\text{Ti}2p}} \times \frac{I_{\text{Ti}2p}^*}{I_{\text{C}1s}^*}}{1 + \frac{I_{\text{C}1s}}{I_{\text{Ti}2p}} \times \frac{I_{\text{Ti}2p}^*}{I_{\text{C}1s}^*} \left\{ 1 - \exp\left(-\frac{a}{\lambda} \cos \vartheta\right) \right\}} \quad (2)$$

$$t = \frac{\lambda}{\cos \vartheta} \ln \left[1 + \frac{I_{\text{C}1s}}{I_{\text{Ti}2p}} \times \frac{I_{\text{Ti}2p}^*}{I_{\text{C}1s}^*} \right] \quad (3)$$

Here, $I_{\text{C}1s}$ and $I_{\text{Ti}2p}$ are the C 1s and Ti 2p intensities, respectively, measured after adsorption of TEOS. The overlayer is assumed to be homogeneous with thickness t and the inelastic mean free paths of the TiO_2 crystal and TEOS overlayer are assumed to be identical. a is an estimate of the lateral length of the TEOS molecules (~ 0.8 nm calculated from DFT the bond lengths), and ϑ is the photoelectron emission angle with respect to the surface normal (0° for all measurements; i.e., all measurements were carried out in normal emission geometry). $I_{\text{C}1s}^*$ and $I_{\text{Ti}2p}^*$ are normalization factors which remove the dependency on the density of the atomic species, subshell photoionization cross section, analyzer and beamline transmission, and the inelastic mean free path at the chosen kinetic energy of the electrons. The ratio is $(I_{\text{Ti}2p}^*/I_{\text{C}1s}^*)a[(N_{\text{Ti}} \sigma_{\text{Ti}2p} T_{\text{Ti}2p}^S \lambda_{\text{Ti}2p} T_{\text{C}1s}^B)/(N_{\text{C}} \sigma_{\text{C}1s} T_{\text{C}1s}^S \lambda_{\text{C}1s} T_{\text{C}1s}^B)]$, where N is the Ti/C atomic density, σ the subshell photoionization cross section of the measured photoelectron line as tabulated in Yeh and Lindau,⁴⁰ T^S the kinetic energy

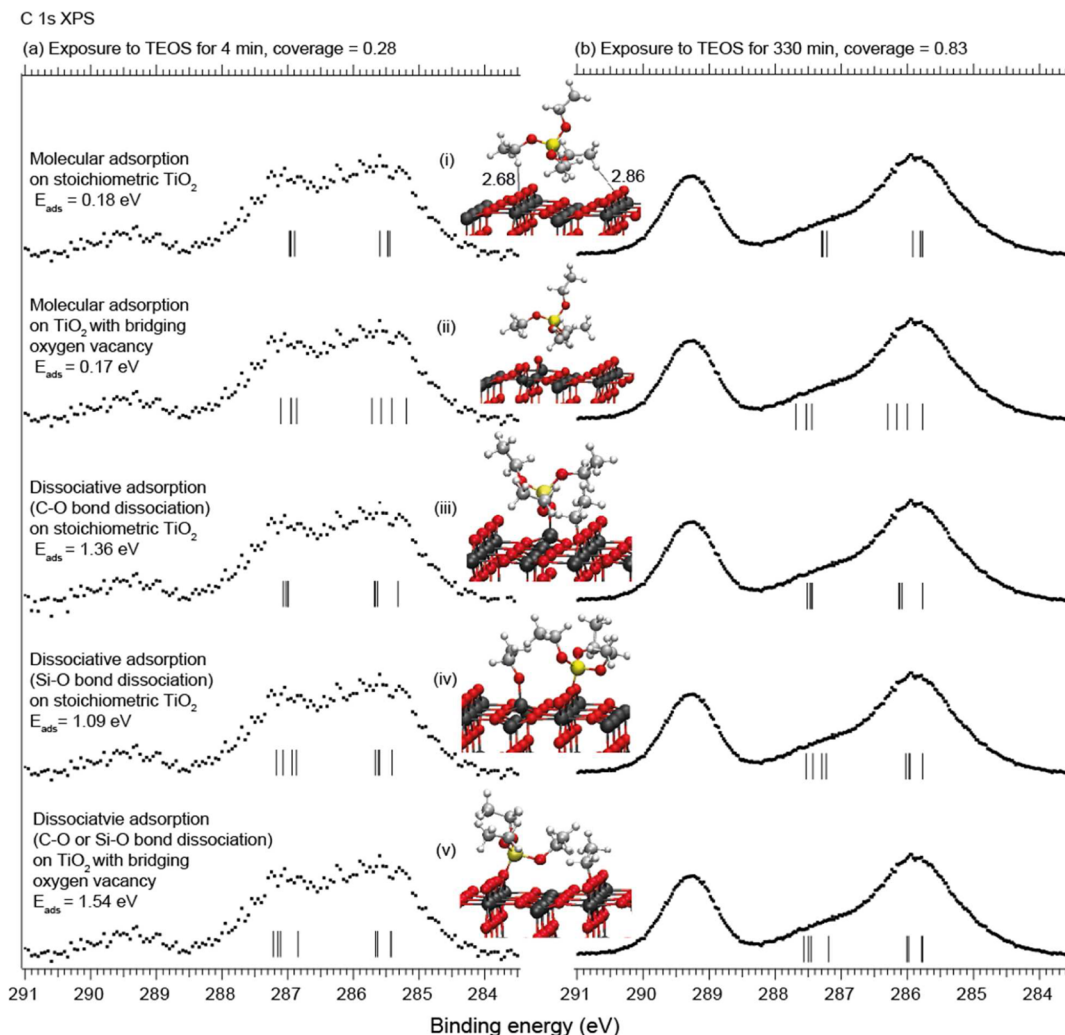


Figure 5. C 1s XP spectra for TEOS exposure of the $\text{TiO}_2(110)$ surface for (a) 4 min and (b) 330 min at room temperature and comparison to calculated binding energy shifts of the geometric models in the middle column (colors, see Figure 2a). In each, the calculated adsorption energy is also given. It should be noted that a reduction of the total energy by adsorption corresponds to a positive adsorption energy.

dependent transmission function of the spectrometer, T^B the photon energy-dependent transmission of the beamline, and λ the inelastic mean free path. We find an N_C value of $0.22 \times 10^{23} \text{ cm}^{-3}$ by assuming a thick film of TEOS with density of $\sim 0.93 \text{ g/cm}^3$ as in the liquid phase^{17,41} and taking into account that one TEOS molecule contains eight carbon atoms. For N_{Ti} we find $0.33 \times 10^{23} \text{ cm}^{-3}$ from the crystal structure of rutile TiO_2 . Since we used the same settings of the electron energy analyzer (slit and pass energy) and the same kinetic energy in the Ti 2p and C 1s measurements, the analyzer transmission factors cancel out as do the mean free path values. The ratio ($T_{\text{Ti}2p}^B/T_{\text{C}1s}^B$) of the beamline transmission factors at the employed photon energies of 560 (Ti 2p measurement) and 390 eV (C 1s) was determined to be ~ 2 from a measurement of the current on a gold mesh introduced in the beamline in front of the end station. For the 4 min deposition of TEOS we find $\theta_A = 0.28$ and $t = 2.25 \text{ \AA}$, where the surface coverage θ_A is defined in terms of the available fivefold-coordinated Ti sites. If we assume that the surface can accommodate one molecule per three surface unit cells, where the unit cell area is $\sim 19.5 \text{ \AA}^2$, $\theta_A = 0.28$ corresponds to approximately 85% of a saturated layer of molecules.

A coverage $\theta_A = 0.125$ was used in the DFT calculations of the initial adsorption, which included calculation of the C 1s binding energy shifts. This coverage was chosen on practical grounds, since it allowed the supercell to be kept to a manageable size, while still being comparable to the lowest experimentally studied coverage. Both the molecular and dissociative adsorption on a perfect surface and a surface holding a bridging oxygen vacancy per supercell, i.e., a 12.5% vacancy concentration, were probed in the calculations. The vacancy concentration is in rough agreement with the spectral intensities in Figure 1, from which we had obtained an upper limit of 14.3% for the bridging oxygen vacancy concentration in Section II.

The middle part of Figure 5 shows the most stable adsorption geometries, in both the absence and the presence of a bridging oxygen vacancy. The adsorption energy for each geometry is indicated. Further, Figure 5a shows a comparison of the experimental C 1s spectra for the initial 4 min deposition of TEOS with the calculated core level shifts. Generally, the lowest binding-energy peak at around 286 eV can be attributed to photoemission from $\text{CH}_3-\text{CH}_2-\text{O}$ and the peak at an intermediate binding energy of around 287.2 eV to $\text{CH}_3-\text{CH}_2-\text{O}$. The peak at a higher energy in the experimental XP

spectrum at approximately 289.2 eV is attributed to a carboxyl species formed after surface reactions. Further surface reactions and thus this particular species have not been taken into account in the calculations, and therefore we will limit here the discussion to the first two peaks of the spectrum. P3 will then be discussed in more detail further below. In all cases the double peak is reproduced, which is because the immediate chemical environment of the photoemitting carbon atoms is not significantly different in the models we have studied. However, the overall shape of the theoretical peaks is very similar in all cases, and it does not allow choosing any of the tested geometries.

Interesting hints come, though, from the computed adsorption energies. It can be seen from Figure 5 that the molecular adsorption of TEOS on both types of surfaces is stable, but only with quite a low adsorption energy (E_{ads}) of 0.18 and 0.17 eV for the perfect and defect-carrying surface, respectively (Figure 5i and ii). The molecular structure is essentially the same in both cases. A higher adsorption energy is found for dissociative adsorption on the stoichiometric surface (Figures 5iii–iv). In the calculations, only one dissociation event per molecule—i.e., the splitting-off of only one and not of multiple ligands—has been taken into account. The two primary dissociation modes of TEOS are by either C–O or Si–O bond breaking.²¹ After C–O bond breaking on the defect-free surface (Figure 5iii) the terminal oxygen atom in TEOS is bound to one fivefold-coordinated Ti atom with a bond distance of 1.84 Å. A secondary interaction is found between the oxygen atom of a second, intact ethoxy ligand and a fivefold-coordinated Ti substrate atom with an interaction length of 2.39 Å. The –CH₂CH₃ residual is adsorbed on a bridging oxygen. In the case of Si–O dissociation (Figure 5iv), the Si atom is bound to a bridging oxygen atom of the surface while the ethoxy is adsorbed on a fivefold-coordinated Ti atom.

The inclusion of an oxygen vacancy in the model results in a further increase of the adsorption energy for dissociative adsorption. After C–O dissociation, the primary residue is adsorbed directly on the vacancy, while the –CH₂CH₃ fragment is bonded to a bridging oxygen atom. After Si–O bond breaking the dissociated ethoxy group is adsorbed directly onto the vacancy while the main residue is bonded to a bridging oxygen atom. Therefore, these two dissociation modes lead to the same final state, which is depicted in Figure 5v. This is indeed the most stable configuration ($E_{\text{ads}} = 1.54$ V) and especially in the low-coverage regime, where we can assume that most of the molecules will react with defects. We conclude therefore that this structure is the most probable one. However, we cannot elucidate which of the possible dissociation pathways are favored, as we do not have information on the reaction barriers for the different processes.

Adsorption of TEOS on TiO₂(110): Low Pressure/Higher Coverage Regime. At a pressure of 5×10^{-9} mbar, TEOS is seen to continuously accumulate on the surface, cf., the C 1s spectra in Figure 3 (cf., also Figure 5b for a comparison to the calculated core level shifts). The spectra are similar to those obtained at lowest coverage, where three peaks were identified as due to photoemission from the terminal methyl groups (CH₃–CH₂–O/P1) at lowest binding energy, oxygen-bonded carbon (CH₃–CH₂–O/P2) at intermediate binding energy, and a high binding energy component P3 assigned to a carboxyl as above. Overall, the intensity increases with exposure time, as illustrated in the inset of Figure 3. Peaks P1 and P2 shift toward higher binding energy, which suggests a

somewhat weakened surface bond of the adsorbates in a more densely packed overlayer. There was no significant effect of band bending which is concluded from a comparison of the valence band for 4 and 330 min exposure time. As before, the intensity of the CH₃–CH₂–O/P1 peak is approximately equal to the sum of the CH₃–CH₂–O/P2 and carboxyl/P3 peak intensities. Nearly the same intensity increase as for the high binding energy peak P3 is seen in the O 1s spectrum in Figure 4, for which we fitted two components (a substrate peak at ~530.6 eV binding energy and a surface bonded ethoxy or carboxylic peak at ~531.9 eV). The difference in energy between the high-energy shoulder and that of the TiO₂(110) support peak is 1.3 eV, which is smaller than what one would expect for an ethoxy species: our DFT calculations show a shift of around 2.0 to 2.3 eV for an ethoxy adsorbate, and Gamble et al. have previously found a difference of around 2.9 eV.¹⁷ However, the shoulder is very broad and could contain a nonresolved component at ~532.6, to be assigned to molecular ethoxy species.

Using eqs 2 and 3 with a beamline transmission ratio ($T_{\text{Ti}2\text{p}}^{\text{B}}/T_{\text{C}1\text{s}}^{\text{B}}$) ≈ 3 rather than 2 due to the use of another monochromator grating, the final coverage and thickness that were obtained during low-pressure exposure, i.e., at an exposure time of 330 min, were found to be 0.99 and 10 Å. Considering the size of the molecules, these values correspond to roughly 3 full molecular layers, i.e., a trilayer. A shift of the C 1s components to a higher binding energy by 0.11 eV due to the decreased core–hole screening efficiency in the multilayer is consistent with the results of the calculation. The size of the shift is within the expected range.^{42,43} It can be noted from the inset in Figure 3 that the growth does not seem to saturate and that further multilayer growth even at low pressure therefore seems feasible, although it was not probed here.

Adsorption of TEOS on TiO₂(110): High Pressure/High Coverage Regime. An increase in TEOS pressure up to around 1 mbar does not bring about any drastic change. Figures 6 and 7 show the C 1s and the Si 2p XP spectra taken for pressures between 10^{-9} and 1.5 mbar. Initially, up to 10^{-1} mbar, gradual shifts toward higher binding energy are observed. The shift in the Si 2p spectrum, which is 0.36 eV in size, is significantly larger than the shift in the C 1s spectrum, which is 0.13 eV. The observation of shifts toward higher binding energy agrees with the formation of a multilayer, although it initially does not grow particularly thick, as is obvious from the only moderate change of the Si 2p and C 1s lines. One can also note that there is a slight change in the peak intensity ratio in disfavor of the high binding energy carboxylic peak. In the high pressure regime around 1 mbar, only the gas-phase lines are visible, which completely suppress the surface signal (Figure 6e and bottom part of Figure 7).

In contrast to the only moderate growth rate at pressures up to $\sim 10^{-1}$ mbar, exposure of the sample to an even higher TEOS pressure at 1 mbar leads to the formation of a thick molecular multilayer. This was observed from the attempted measurement of a Ti 2p XP spectrum after 1 mbar exposure. No Ti 2p intensity was observable. In addition, the C 1s spectrum was modified in comparison to the spectra taken before exposure at 1 mbar: the separation between the C 1s CH₃–CH₂–O/P1 and CH₃–CH₂–O/P2 components increased from 1.46 to ~ 1.7 eV, and the intensity ratio between the CH₃–CH₂–O/P1 and carboxyl/P3 peaks changed (cf., the C 1s spectrum at 300 K in Figure 8a).

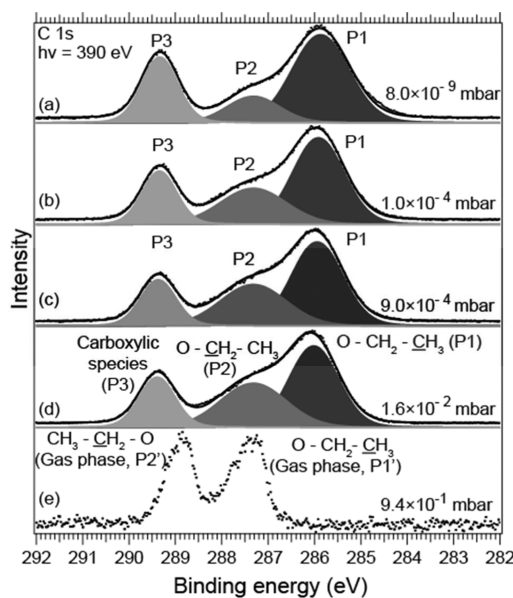


Figure 6. C 1s spectra recorded during exposure of the $\text{TiO}_2(110)$ to the indicated pressure of TEOS at room temperature: (a) 8.0×10^{-9} , (b) 1.0×10^{-4} , (c) 9.0×10^{-4} , and (d) at 1.6×10^{-2} mbar. Peak P1 is attributed to terminal methyl groups ($\text{CH}_3-\text{CH}_2-\text{O}$), P2 to oxygen-bonded carbon ($\text{CH}_3-\underline{\text{CH}_2}-\text{O}$), and P3 to a surface-bonded carboxyl species. The spectra are normalized to their maximum height. (e) Gas-phase spectrum of TEOS at 9.4×10^{-1} mbar (cf., Figure 2b). (Refer to Table 1 for binding energies and intensity ratios.)

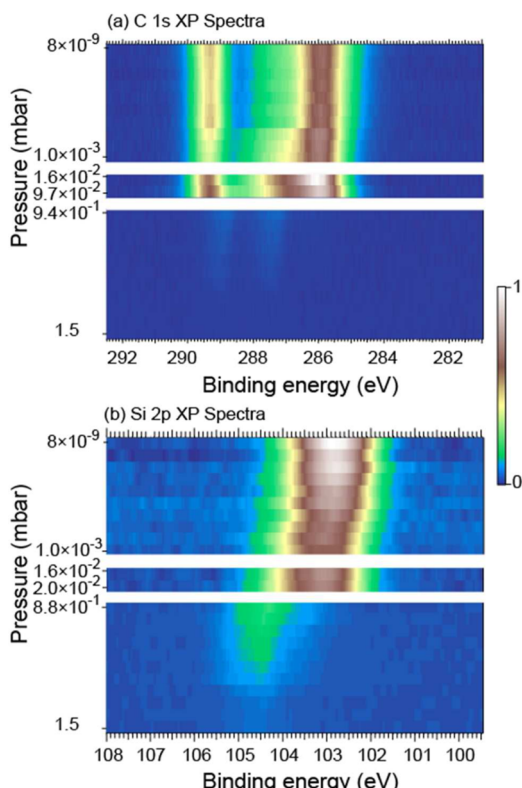


Figure 7. (a) C 1s and (b) Si 2p spectra measured during exposure of the $\text{TiO}_2(110)$ to the indicated pressures of TEOS. At a pressure of $\sim 9 \times 10^{-1}$ mbar the peak shifts significantly toward higher binding toward the location of the gas-phase peak (in other words, the solid state contribution is dominated by that of the gas phase). The color scale represents the intensity of the peaks.

Table 1. Binding Energies and Intensity Ratios of the Components in the C 1s XP Spectra in Figure 6^a

pressure (mbar)	binding energy of components (eV)			intensity ratio	
	P1	P2	P3	P2/P1	P3/P1
8.0×10^{-9}	285.87	287.32	289.34	0.28	0.48
1.0×10^{-4}	285.92	287.32	289.36	0.53	0.42
9.0×10^{-4}	285.94	287.32	289.36	0.63	0.39
1.6×10^{-2}	286.02	287.32	289.38	0.71	0.45

^aThe values were obtained by least-squares curve fitting. All binding energies have an error of ± 0.1 eV.

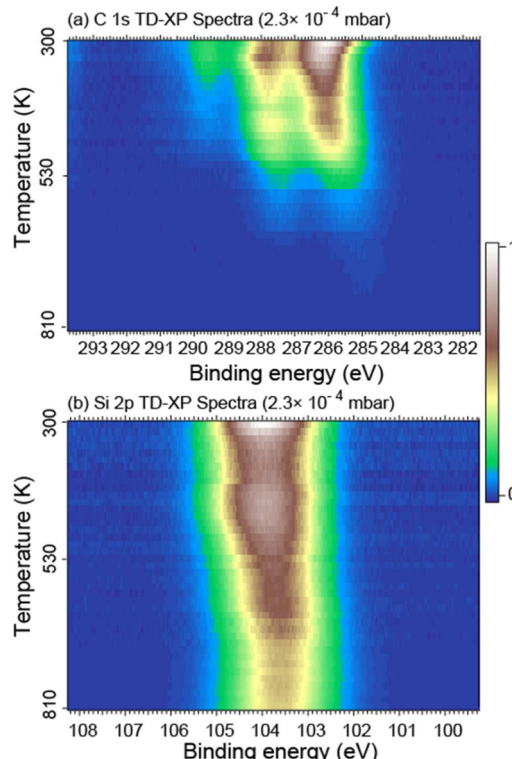


Figure 8. (a) C 1s and (b) Si 2p TDXPS measurements performed on a multilayer of TEOS on $\text{TiO}_2(110)$ obtained after exposure of crystal to vapor pressure of TEOS. The pressure during the present measurements was 2.3×10^{-4} mbar. Peak P3 in the C 1s spectra vanishes at around 500 K, while the surface ethoxysilyl peaks remains until 650 K (cf., Figure 13). At 800 K, these components also disappear, whereas the Si 2p persists. The color scale gives the intensity.

SiO₂ Growth by CVD. To study the CVD process, a series of temperature-dependent XPS (TDXPS) experiments were conducted at a TEOS pressure of 2.3×10^{-4} mbar. During this temperature increase, C 1s and Si 2p XP spectra were collected (Figure 8). Clearly, a reduction of intensity is seen for all monitored components. The carboxyl/P3 peak in the C 1s spectrum was the first component to completely disappear, a process which is finished at around 500 K. The other two C 1s components persist until a higher temperature but vanish completely well before the temperature reached 800 K. In contrast, the Si 2p line remains for all temperatures, albeit with a clear reduction in intensity: the C 1s/Si 2p intensity ratio for the multilayer of TEOS at room temperature is 2.17, while it decreases to 0.01 at 800 K. This shows that all ethoxy groups leave the surface, presumably as ethylene and ethanol,¹⁷ but

probably also in carbonyl form (specifically as acetaldehydes).⁴⁴ Acetaldehyde was reported as one of the significant reaction products of ethanol on TiO_2 nanoparticles and single crystal surfaces at temperatures 473 to 610 K.^{45–47} The intensity ratio of the Si 2p line at 800 K to that at 300 K is 0.47, which provides a lower limit for the desorption of Si: first ignoring that the Si 2p intensity would be affected positively by the desorption of ligands, the ratio would imply disappearance of nearly half of the ethoxysilyl groups present in the multilayer at 300 K. The factual ratio of desorption must be higher due to the negative influence of the presence of ligands on the Si 2p intensity due to photoelectron attenuation. In any case, it is clear that only silicon in close contact with the surface survives to 800 K. This surviving Si species has a lower Si 2p binding energy with a shift of 0.33 eV with respect to the initial multilayer species (Figure 8b). This shift is too small to assign to any other suboxides, which usually have shifts of ~ 0.8 for Si^{3+} and ~ 1.5 for Si^{2+} .⁴⁸

An O 1s spectrum (Figure 9a) was taken at the end of the first TD-XPS run at 800 K, at which the Si 2p peak was seen to

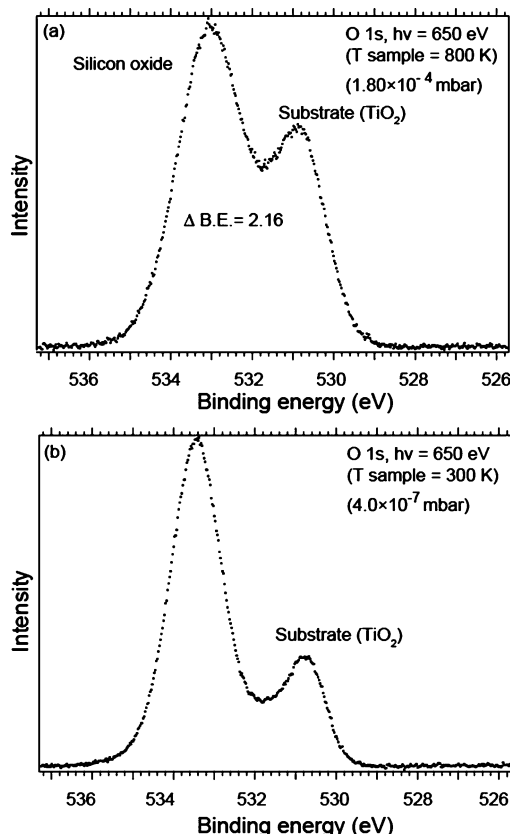


Figure 9. O 1s XP spectra at (a) 800 K and (b) cooled to 300 K after heating the surface to 800 K. The change in intensity ratio is due to the room temperature adsorption of residual gas molecules at a pressure of 4.0×10^{-7} mbar.

still be present (Figure 8b). The presence of only Si and O at the surface suggests formation of silicon oxide at this temperature. The binding energy of the SiO_2 -related component in the O 1s XP spectrum is by ~ 2.1 eV higher than that of the TiO_2 -component in agreement with literature values.^{49–52} After the measurement, the surface was allowed to cool to room temperature and another O 1s spectrum was taken (Figure 9b). The change in line shape, together with a

decrease of the Si 2p:Ti 2p intensity ratio from 1.93 to 3.54, clearly shows adsorption of residual molecules on the surface. Indeed, the pressure remained at 4.0×10^{-7} mbar. Also, the appearance of the C 1s spectrum measured under these conditions (Figure S2 in Supporting Information) confirms the presence of chemisorbed molecules at the surface.

The TDXPS experiment was repeated in a second run, this time at lower pressure, 2.3×10^{-7} mbar. During this second TDXPS run the O 1s and Si 2p lines were recorded and are shown in Figure 10. Clearly, the TiO_2 -related O 1s peak has a

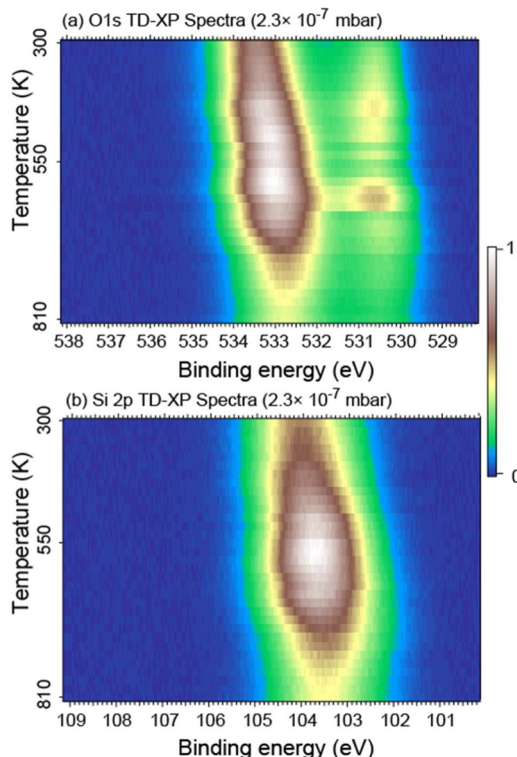


Figure 10. (a) O 1s (a) and (b) Si 2p TD-XP spectra for TEOS adsorbed on the silicon oxide layer grown on the TiO_2 (110) surface in the first TDXPS experiment. The color scale represents the intensity of peaks.

constant binding energy (at ~ 530.6 eV), while the adsorption/reaction-induced peak (around 533 eV) moves down in binding energy by ~ 0.4 eV (Figure 10a). The downward shift of the adsorption/reaction-induced peak is attributed to the dissociation of molecules resulting in the formation of silicon oxide. We can also note the presence of a shoulder in the O 1s spectra at 532.0 eV at intermediate temperature. The Si 2p line is found to shift down in binding energy, in line with the results for the first TDXPS run. Moreover, it is seen to first increase in intensity, in agreement with ligand desorption, but to also lose intensity at higher temperatures. Hence, Si is lost from the sample surface, either by desorption or by bulk migration.

Figure 11 compares the final O 1s spectra of the two TDXPS experiments. Clearly, the signal related to the TiO_2 support is reduced in intensity after the second run. In line with the hypothesis of SiO_2 formation, we therefore suggest that additional silicon oxide was formed also in the second TDXPS experiment at lower pressure.

Finally, an AFM image was taken on the crystal after the second TDXPS run and compared to that of a clean TiO_2 (110) crystal (Figure 12). The measurements were performed in air,

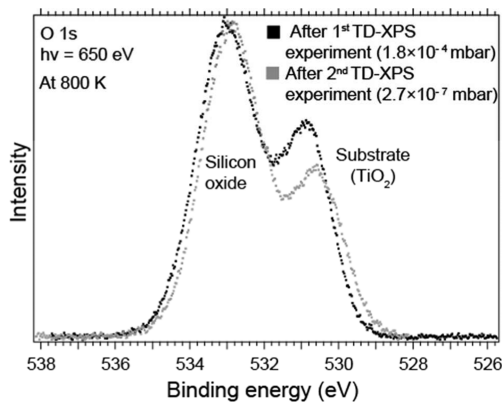


Figure 11. Comparison of the O 1s XP spectra after first (black) and second (gray) TDXPS experiments. Clearly, the silicon dioxide peak has increased in intensity, which reflects the growth of silicon oxide in the second TD-XPS experiment.

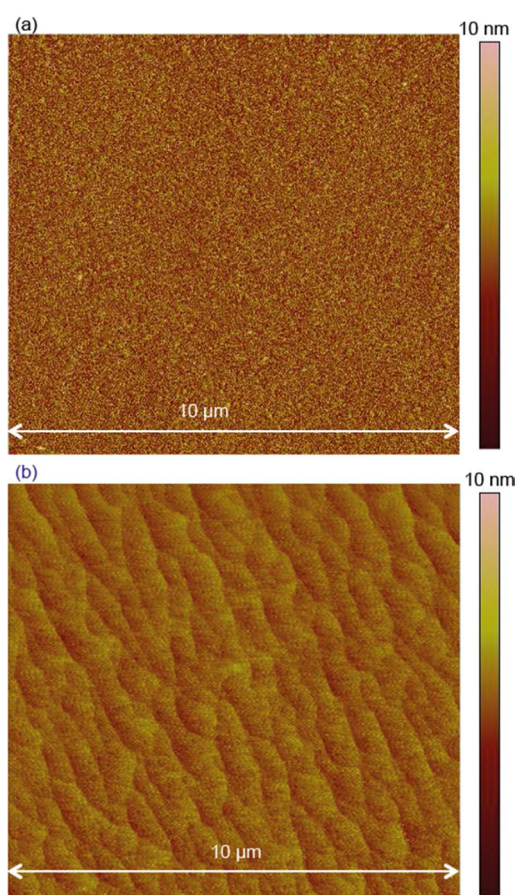


Figure 12. AFM images of (a) a clean $\text{TiO}_2(110)$ surface and of (b) the silicon dioxide layer formed on the $\text{TiO}_2(110)$ single crystal surface in the second TDXPS experiment.

which prevented atomic resolution. Clearly, the appearance of the surface was modified quite strongly, in line with the hypothesis of silicon dioxide formation. The typical length of structure observed in a clean $\text{TiO}_2(110)$ surface is $0.18 \mu\text{m}$ and for silicon oxide grown surface it is $0.65 \mu\text{m}$.

IV. DISCUSSION

Room Temperature Adsorption. First we note that the present results could have been influenced by the presence of

residual water in the preparation chamber of the experimental station and hence the hydroxylation of the $\text{TiO}_2(110)$ surface, since the base pressure in the chamber was 5×10^{-9} mbar. Hydroxyl groups on the surface do not affect the results in a significant way, since, as already proposed by Gamble and as confirmed by the present results, TEOS adsorbs dissociatively—with the splitting-off of ligands and binding of the ligands to the surface as ethoxy groups—on both the hydroxylated and nonhydroxylated $\text{TiO}_2(110)$ surfaces.¹⁷

It is not straightforward to distinguish in the C 1s XP signals from ethoxy ligands that remain bonded to the Si atom upon adsorption of the molecule on the surface and those from ethoxy ligands that are split off by Si–O bond breaking and bind to either the fivefold-coordinated Ti atoms of the surface or bridging oxygen vacancies^{17,53} or even to ethoxy formed via C–O bond breaking with ethyl bonded to bridging oxygen atoms: in all three cases, peaks P1 and P2 are expected in a 1:1 intensity ratio in the C 1s spectrum approximately at the binding energies observed here. It is clear, however, that the adsorption process of TEOS under the present conditions must differ from this simple case: the deviation from the 1:1 intensity ratio of the P1 and P2 peaks seen in Figure 3—the intensity ratio is 0.28—suggests that a surface reaction beyond pure ligand split-off takes place. This surface reaction should be related to the occurrence of the high-binding energy peak in the C 1s XP spectra with a binding energy typically found for carboxyl species. This hypothesis is substantiated by the finding that the intensity ratio of P1 to the sum of P2 and P3 is 1 for all room-temperature C 1s spectra; hence, any model of room temperature adsorption should contain as an ingredient the preservation of terminal methyl groups, while the nature of the oxygen-bonded carbon is changed in the reaction. These findings can be reconciled when noting that TiO_2 -bonded ethoxy groups can be converted into surface-bonded acetaldehyde and deprotonated acetic acid, with intact terminal methyl groups, by dehydrogenation.^{44,54} Indeed, conversion of surface-bonded ethoxy into carboxyl species has been observed before, but has been said to require illumination by UV light.^{22,55} Closer inspection of the C 1s data in these previous works as well as in a work on ethanol adsorption⁵⁶ on $\text{TiO}_2(110)$ suggest the presence of a smaller carboxyl component already before UV irradiation, which is in line with what is reported here.

A possible reaction scheme for the conversion of the ethoxy to carboxyl species is depicted in Figure 13, for both the stoichiometric $\text{TiO}_2(110)$ surface and that with a bridging oxygen vacancy, which acts as the reaction center. As previously reported, the initial adsorption entails a dissociative adsorption resulting in ethyl and ethoxy groups according to the scheme in Figure 13. These groups could undergo further dehydrogenation steps when reacting with bridging oxygen atoms and hydroxyls. In Figure 13 it is assumed that no previous water adsorption has taken place, which entails complete absence of surface hydroxyls on both the fivefold-coordinated Ti atoms and the bridging oxygen atoms. Even then, bridging oxygen hydroxyls would be formed by all dehydrogenation pathways, which then could assist in the further dehydrogenation according to the bottom part of the figure. The possible presence of residual water, leading to the creation of hydroxyls on the fivefold-coordinated Ti atoms, would open further reaction pathways, but at the same time it probably would lead to the closure of the pathways involving bridging oxygen vacancies, since it is known that the vacancies are filled by

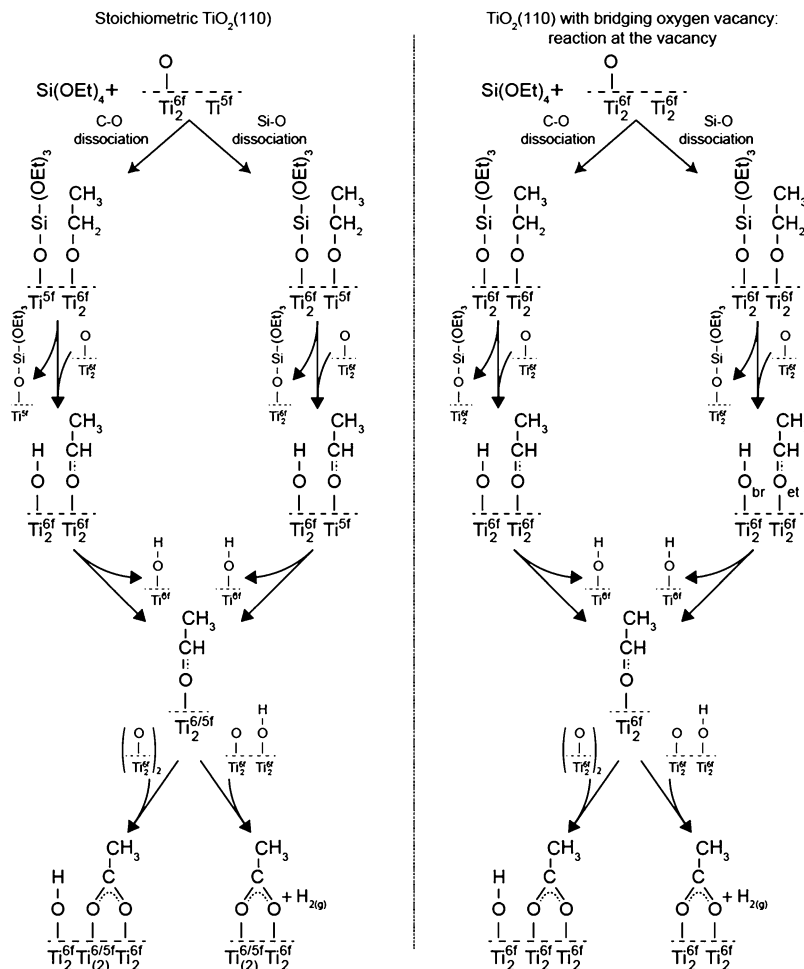


Figure 13. Initial dissociation of the TEOS followed by surface reactions to acetaldehyde and possibly deprotonated acetic acid. Only pathways in the absence of hydroxyls on the fivefold-coordinated Ti atoms have been considered. Ti^{sf} represents the fivefold-coordinated Ti atoms, while Ti_2^{sf} represents the two sixfold-coordinated Ti atoms bonded to a bridging oxygen atom or adjacent to a vacancy, while $\text{Ti}_2^{\text{sf}}(2)$ stands for both kinds of site. The subscript (g) denotes a gas-phase molecule.

water. In any case, it is clear that pathways exist that lead to the formation of a carboxylate in agreement with the observation of the P3 peak in the C 1s spectra with an energy that is within the correct range for a carboxylate.^{54,55} Even the increased formation of the carboxyl species can be rationalized in this scheme: the initial dehydrogenation of the surface-bonded ethyl group will lead to formation of bridging oxygen hydroxyls, which can lead to an increased rate of carboxylate formation. Also, intermolecular interactions at higher coverage could play an important role in the increased tendency to form carboxylates.

At this place we would like to reiterate what we have stated in both the *Methods* and *Results* sections above, namely, that a fraction of, but clearly not the entire, intensity of the carboxyl P3 peak is likely to be related to a photoinduced reaction, i.e., to beam damage. The data for APTES, a compound with very similar chemistry as that of TEOS, in the *Supporting Information* make clear that a significant part of the P3 intensity indeed is related to the surface chemistry of TEOS and ethoxides on the $\text{TiO}_2(110)$ surface. As has been stated above, similar peaks are seen in previously reported XP spectra of ethanol adsorbed on the $\text{TiO}_2(110)$ surface obtained on surfaces not irradiated by UV light.^{22,56} However, the peaks have not been discussed any further. The varying intensity of

this carboxyl feature could possibly suggest that the conversion rate depends strongly on the exact chemical state of the surface, which can vary quite strongly with crystal manufacturer, between different batches from the same manufacturer, and with the exact surface cleaning protocol.

A significant difference of the present in comparison to these previous studies, as well as that on the adsorption of TEOS on $\text{TiO}_2(110)$ by Gamble et al.,¹⁷ who did not observe conversion of surface ethoxy into carboxyl groups, lies in the fact that here TEOS always was readily available for adsorption and readsorption due to either the residual pressure of TEOS or the deliberate exposure to higher pressures. This was not the case in the previously reported experiments, which were carried out in a post mortem fashion. In the particular case of TEOS adsorption on $\text{TiO}_2(110)$, Gamble et al. found a significant difference in fourfold-coordinated Ti-bonded ethoxy groups and those bonded to bridging oxygen vacancies.⁵³ The latter were significantly more stable and reacted first at around 500 K, while the former desorbed from the surface at temperatures between 250 and 400 K. However, Gamble et al. suggested the Si–O bond breaking mechanism on nearly perfect $\text{TiO}_2(110)$ on the basis of equal peak intensity for P1 and P2, which also holds for C–O dissociation. As in case of C–O dissociation the ethyl bonded to a bridging oxygen will also give the same peak

intensity ratio and is also favored with low adsorption energy of 1.36 eV on a perfect surface (Figure 5c).

It is interesting to see that the carboxyl species with the high binding energy fingerprint in the C 1s spectra is also found in the thick multilayer (cf., Figure 8a, room temperature). This suggests that there exist reaction paths toward the formation of carboxyl species even in the multilayer. Since the rate of beam damage in a thick film of TEOS might differ significantly from that in a thin film, we cannot exclude, however, that the formation of such a carboxyl species in the multilayer is entirely related to beam damage.

SiO₂ Growth by CVD. Turning to the CVD growth probed in TDXPS, it is observed that the carboxyl species is most loosely bound to the surface of all TEOS-derived adsorbates; it desorbs at temperatures below 500 K, while the species related to the P1 and P2 components in the C 1s spectra persist to significantly higher temperatures. Further, it is seen that the P1 and P2 peaks are almost the same after desorption of the carboxyl species and that they follow the same desorption pattern at high temperature (Figure 14 and Figure S3 in the

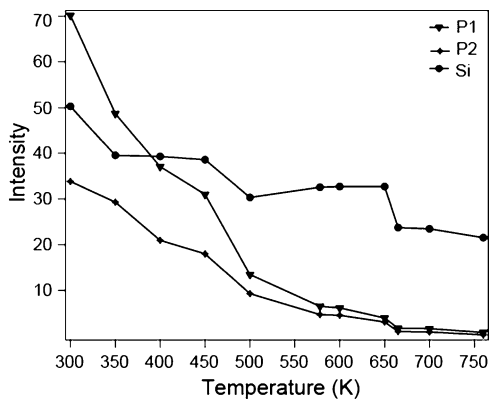


Figure 14. Intensities of the P1 and P2 peaks in the C 1s spectra during the first TD-XPS experiment together with the intensity of the Si 2p spectra.

Supporting Information. This suggests that the molecular species that survives to higher temperatures is an ethoxy or ethyl species, although it remains unclear whether it is Si- or Ti-bonded, or whether both types occur. The Si 2p intensity decreases roughly by a factor of 2, and hence Si is desorbed from the surface during the temperature run. The remaining Si species form SiO₂ as outlined earlier. The observation of the high binding energy component in the O 1s XP spectra agrees with this hypothesis.⁵³ The appearance of the AFM images lends further support.

Finally, in the second TD-XPS experiment a shoulder was observed in the O 1s XP spectra intermediate in binding energy between that of the SiO₂- and that of the TiO₂-related peak (in the first TD-XPS run no O 1s spectra were recorded. It seems likely that this peak, which occurs at intermediate temperatures, is related to a mixed oxide of titanium and silicon which is in accordance with literature studies.^{49,50,57} In particular, a systematic study by Sun et al.⁴⁹ shows the formation of mixed oxide with different concentration of precursors (titanium isopropoxide for TiO₂ and TEOS for SiO₂), which confirms the assignment of the peak intermediate in binding energy in the O 1s spectrum after the second TD-XPS experiment to a mixed oxide of Ti-Si. Its disappearance at high

temperature could be due to the migration of into the bulk of the crystal.

V. CONCLUSIONS

In the present work we have studied, using UHV and near-ambient XPS and DFT, the adsorption of TEOS on the rutile TiO₂(110) surface at limited TEOS doses and how the adsorption behavior is modified by the presence of a TEOS gas-phase reservoir. We have also studied the CVD growth of silicon oxide on TiO₂(110) from TEOS using NAPXPS. XPS and DFT provide evidence for the dissociative adsorption of TEOS on the TiO₂(110) surface at room temperature. The availability of TEOS in the gas phase changes the surface processes significantly and moves the equilibrium of the surface reaction toward the formation of a carboxyl species and away from the simple binding of ethoxy groups. Upon heating, the molecular layer is transformed into SiO₂ in a CVD process, which was followed in real time by NAPXPS as well as in a post mortem AFM experiment. An oxygen species intermediate in O 1s binding energy between the lines due to SiO₂ and TiO₂ is found during the SiO₂ CVD at a temperature of around 600 K. This species is tentatively assigned to a mixed titanium/silicon oxide. The present study shows the potential of NAPXPS for the real-time monitoring of CVD and ALD, which can help in understanding the surface chemistry of these processes and thus eventually lead to improved protocols and a high control of the quality of thin layers grown by CVD and ALD.

■ ASSOCIATED CONTENT

S Supporting Information

The Supporting Information is available free of charge on the ACS Publications website at DOI: 10.1021/acs.jpcc.5b04985.

Formulas for the calculation of bridging oxygen vacancy concentration, C 1s XP spectra after the TD-XPS experiment and at 650 K during first TDXPS experiment (PDF)

■ AUTHOR INFORMATION

Corresponding Author

* E-mail: joachim.schnadt@sljus.lu.se. Tel.: +46 46-222 3925.

Author Contributions

The manuscript was written through contributions of all authors. All authors have given approval to the final version of the manuscript.

Notes

The authors declare no competing financial interest.

■ ACKNOWLEDGMENTS

The authors would like to acknowledge financial support from the European Commission via the Initial Training Network SMALL (MCITN-238804) and the Swedish Research Council (VR) (grant nos. 2010-5080 and 2014-3776).

■ REFERENCES

- Jones, A. C.; Hitchman, M. L. *Chemical Vapour Deposition: Precursors, Processes and Applications*; Royal Society of Chemistry: Cambridge, 2009.
- Zaera, F. Mechanisms of Surface Reactions in Thin Solid Film Chemical Deposition Processes. *Coord. Chem. Rev.* 2013, 257, 3177–3191.
- Taylor, C. J.; Gilmer, D. C.; Colombo, D. G.; Wilk, G. D.; Campbell, S. A.; Roberts, J.; Gladfelter, W. L. Does Chemistry Really

- Matter in the Chemical Vapor Deposition of Titanium Dioxide? Precursor and Kinetic Effects on the Microstructure of Polycrystalline Films. *J. Am. Chem. Soc.* **1999**, *121*, 5220–5229.
- (4) Sandell, A.; Andersson, M. P.; Johansson, M. K.-J.; Karlsson, P. G.; Alfredsson, Y.; Schnadt, J.; Siegbahn, H.; Uvdal, P. Metalorganic Chemical Vapor Deposition of Anatase Titanium Dioxide on Si: Modifying the Interface by Pre-oxidation. *Surf. Sci.* **2003**, *530*, 63–70.
- (5) Karlsson, P. G.; Richter, J. H.; Andersson, M. P.; Johansson, M. K.-J.; Blomquist, J.; Uvdal, P.; Sandell, A. TiO₂ Chemical Vapor Deposition on Si(111) in Ultrahigh Vacuum: Transition from Interfacial Phase to Crystalline Phase in the Reaction Limited Regime. *Surf. Sci.* **2011**, *605*, 1147–1156.
- (6) Mannie, G. J. A.; Gerritsen, G.; Abbenhuis, H. C. L.; van Deelen, J.; Niemantsverdriet, J. W.; Thüne, P. C. X-ray Photoelectron Spectroscopy Study on the Chemistry Involved in Tin Oxide Film Growth during Chemical Vapor Deposition Processes. *J. Vac. Sci. Technol., A* **2013**, *31*, 01A105.
- (7) Huang, M. L.; Chang, Y. H.; Lin, T. D.; Lin, H. Y.; Liu, Y. T.; Pi, T. W.; Hong, M.; Kwo, J. Growth Mechanism of Atomic Layer Deposited Al₂O₃ on GaAs(001)-4 × 6 Surface with Trimethylaluminum and Water as Precursors. *Appl. Phys. Lett.* **2012**, *101*, 212101.
- (8) Starr, D. E.; Liu, Z.; Hävecker, M.; Knop-Gericke, A.; Bluhm, H. Investigation of Solid/Vapor Interfaces using Ambient Pressure X-ray Photoelectron Spectroscopy. *Chem. Soc. Rev.* **2013**, *42*, 5833–5857.
- (9) Rupprechter, G. Sum Frequency Laser Spectroscopy during Chemical Reactions on Surfaces. *MRS Bull.* **2007**, *32*, 1031–1037.
- (10) Peters, S. J.; Ewing, G. E. Water on Salt: An Infrared Study of Adsorbed H₂O on NaCl(100) under Ambient Conditions. *J. Phys. Chem. B* **1997**, *101*, 10880–10886.
- (11) Oroshnik, J.; Kraitchman, J. Pyrolytic Deposition of Silicon Dioxide in an Evacuated System. *J. Electrochem. Soc.* **1968**, *115*, 649–652.
- (12) Crowell, J. E.; Tedder, L. L.; Cho, H.-C.; Casciaro, F. M.; Logan, M. A. Model Studies of Dielectric Thin Film Growth: Chemical Vapor Deposition of SiO₂. *J. Vac. Sci. Technol., A* **1990**, *8*, 1864–1870.
- (13) Rauscher, H. The Interaction of Silanes with Silicon Single Crystal Surfaces: Microscopic Processes and Structure. *Surf. Sci. Rep.* **2001**, *42*, 207–328.
- (14) Gallas, B.; Brunet-Bruneau, A.; Fisson, S.; Vuye, G.; Rivory, J. SiO₂–TiO₂ Interfaces Studied by Ellipsometry and X-ray Photoemission Spectroscopy. *J. Appl. Phys.* **2002**, *92*, 1922–1928.
- (15) Houmard, M.; Riassetto, D.; Roussel, F.; Bourgeois, A.; Berthomé, G.; Joud, J. C.; Langlet, M. Enhanced Persistence of Natural Super-Hydrophilicity in TiO₂–SiO₂ Composite Thin Films Deposited via a Sol–Gel route. *Surf. Sci.* **2008**, *602*, 3364–3374.
- (16) Niphadkar, P. S.; Chitale, S. K.; Sonar, S. K.; Deshpande, S. S.; Joshi, P. N.; Awate, S. V. Synthesis, Characterization and Photocatalytic Behavior of TiO₂–SiO₂ Mesoporous Composites in Hydrogen Generation from Water Splitting. *J. Mater. Sci.* **2014**, *49*, 6383–6391.
- (17) Gamble, L.; Hugenschmidt, M. B.; Campbell, C. T.; Jurgens; Teresa, A.; Rogers, J. W. Adsorption and Reactions of Tetraethoxysilane (TEOS) on Clean and Water-Dosed Titanium Dioxide (110). *J. Am. Chem. Soc.* **1993**, *115*, 12096–12105.
- (18) Polack, F.; Silly, M.; Chauvet, C.; Lagarde, B.; Bergeard, N.; Izquierdo, M.; Chubar, O.; Krizmancic, D.; Ribbens, M.; Duval, J.-P.; et al. TEMPO: A New Insertion Device Beamline at SOLEIL for Time Resolved Photoelectron Spectroscopy Experiments on Solids and Interfaces. *AIP Conf. Proc.* **2010**, *185*, 185–188.
- (19) Wendt, S.; Schaub, R.; Matthiesen, J.; Vestergaard, E. K.; Wahlström, E.; Rasmussen, M. D.; Thostrup, P.; Molina, L. M.; Lægsgaard, E.; Stensgaard, I.; et al. Oxygen Vacancies on TiO₂(110) and their Interaction with H₂O and O₂: A Combined High-Resolution STM and DFT study. *Surf. Sci.* **2005**, *598*, 226–245.
- (20) Olivero, J.; Longbothum, R. Empirical Fits to the Voigt Line Width: A Brief Review. *J. Quant. Spectrosc. Radiat. Transfer* **1977**, *17*, 233–236.
- (21) Gallet, J.-J.; Bournel, F.; Pierucci, D.; Bonato, M.; Khalil, A.; Rochet, F.; Silly, M.; Sirotti, F. A Synchrotron Radiation X-ray Photoemission Spectroscopy Study of *n*-Propyltriethoxysilane Adsorption on Si(001)-2 × 1 at Room Temperature. *J. Phys. Chem. C* **2010**, *114*, 21450–21456.
- (22) Jayaweera, P. M.; Quah, E. L.; Idriss, H. Photoreaction of Ethanol on TiO₂(110) Single-Crystal Surface. *J. Phys. Chem. C* **2007**, *111*, 1764–1769.
- (23) Kresse, G.; Hafner, J. Ab Initio Molecular Dynamics for Liquid Metals. *Phys. Rev. B: Condens. Matter Mater. Phys.* **1993**, *47*, 558–561.
- (24) Kresse, G.; Hafner, J. Ab Initio Molecular-Dynamics Simulation of the Liquid-Metal-Amorphous Semiconductor Transition in Germanium. *Phys. Rev. B: Condens. Matter Mater. Phys.* **1994**, *49*, 14251–14269.
- (25) Kresse, G.; Furthmüller, J. Efficiency of Ab-Initio Total Energy Calculations for Metals and Semiconductors Using a Plane-Wave Basis set. *Comput. Mater. Sci.* **1996**, *6*, 15–50.
- (26) Kresse, G.; Furthmüller, J. Efficient Iterative Schemes for Ab Initio Total-Energy Calculations using a Plane-Wave Basis Set. *Phys. Rev. B: Condens. Matter Mater. Phys.* **1996**, *54*, 11169–11186.
- (27) Perdew, J. P.; Burke, K.; Ernzerhof, M. Generalized Gradient Approximation Made Simple. *Phys. Rev. Lett.* **1996**, *77*, 3865–3868.
- (28) Perdew, J. P.; Burke, K.; Ernzerhof, M. Erratum: Generalized Gradient Approximation Made Simple. *Phys. Rev. Lett.* **1997**, *78*, 1396–1396.
- (29) Blochl, P. E. Projector Augmented-Wave Method. *Phys. Rev. B: Condens. Matter Mater. Phys.* **1994**, *50*, 17953–17979.
- (30) Kresse, G.; Joubert, D. From Ultrasoft Pseudopotentials to the Projector Augmented-Wave Method. *Phys. Rev. B: Condens. Matter Mater. Phys.* **1999**, *59*, 1758–1775.
- (31) Monkhorst, H. J.; Pack, J. G. Special Points for Brillouin-Zone Integrations. *Phys. Rev. B* **1976**, *13*, 5188–5192.
- (32) Mortensen, J. J.; Hansen, L. B.; Jacobsen, K. W. Real-Space Grid Implementation of the Projector Augmented Wave Method. *Phys. Rev. B: Condens. Matter Mater. Phys.* **2005**, *71*, 035109.
- (33) Enkovaara, J.; Rostgaard, C.; Mortensen, J. J.; et al. Electronic Structure Calculations with GPAW: A Real Space Implementation of the Projector Augmented-Wave Method. *J. Phys.: Condens. Matter* **2010**, *22*, 253202.
- (34) Bahn, S. R.; Jacobsen, K. W. An Object-Oriented Scripting Interface to a Legacy Electronic Structure Code. *Comput. Sci. Eng.* **2002**, *4*, 56–66.
- (35) Ljungberg, M. P.; Mortensen, J. J.; Pettersson, L. G. M. An Implementation of Core Level Spectroscopies in a Real Space Projector Augmented Wave Density Functional Theory Code. *J. Electron Spectrosc. Relat. Phenom.* **2011**, *184*, 427–439.
- (36) Nagao, M.; Yamashita, Y.; Machida, S.; Hamaguchi, K.; Yasui, F.; Mukai, K.; Yoshinobu, J. Nature of Interface Bonding of Ethylene and Benzene with Si(100)c(4 × 2): Angle-Dependent Si 2p High Resolution Photoelectron Spectroscopy Studies. *Surf. Sci.* **2002**, *513*, 413–421.
- (37) Briggs, D.; Beamson, G. Primary and Secondary Oxygen-Induced C1s Binding Energy Shifts in X-ray Photoelectron Spectroscopy of Polymers. *Anal. Chem.* **1992**, *64*, 1729–1736.
- (38) Ertl, G.; Küppers, J. Low Energy Electrons and Surface Chemistry, 2nd ed.; VCH: Weinheim, 1986; pp 75–78.
- (39) Streubel, P.; Hesse, R.; Makhova, L.; Schindelka, J.; Denecke, R. A Practicable Method for Thickness Estimation of Ultrathin Layers from XPS Data with UNIFIT 2011; Technical Report; University of Leipzig, Germany, 2011.
- (40) Yeh, J. J.; Lindau, I. Atomic Subshell Photoionization Cross Sections and Asymmetry Parameters: 1 ≤ Z ≤ 103. *At. Data Nucl. Data Tables* **1985**, *32*, 1–155.
- (41) Misra, A.; Hogan, J. D.; Chorush, R. Teos. *Handbook of Chemicals and Gases for the Semiconductor Industry*; Wiley-VCH: New York, 2002.
- (42) Isvoranu, C.; Åhlund, J.; Wang, B.; Ataman, E.; Mårtensson, N.; Puglia, C.; Andersen, J. N.; Bocquet, M.-L.; Schnadt, J. Electron Spectroscopy Study of the Initial Stages of Iron Phthalocyanine

Growth on Highly Oriented Pyrolytic Graphite. *J. Chem. Phys.* **2009**, *131*, 214709.

(43) Maxwell, A. J.; Brühwiler, P. A.; Arvanitis, D.; Hasselström, J.; Mårtensson, N. C 1s Ionisation Potential and Energy Referencing for Solid C₆₀ Films on Metal Surfaces. *Chem. Phys. Lett.* **1996**, *260*, 71–77.

(44) Farfan-Arribas, E.; Madix, R. J. Role of Defects in the Adsorption of Aliphatic Alcohols on the TiO₂ (110) surface. *J. Phys. Chem. B* **2002**, *106*, 10680–10692.

(45) Kim, K. S.; Barteau, M. A.; Farneth, W. E. Adsorption and Decomposition of Aliphatic Alcohols on TiO₂. *Langmuir* **1988**, *4*, 533–543.

(46) Idriss, H.; Seebauer, E. G. Reactions of Ethanol over Metal Oxides. *J. Mol. Catal. A: Chem.* **2000**, *152*, 201–212.

(47) Kim, K. S.; Barteau, M. A. Reactions of Aliphatic Alcohols on the {011}-Faceted TiO₂ (001) Surface. *J. Mol. Catal.* **1990**, *63*, 103–117.

(48) Tissot, H.; Gallet, J.-J.; Bournel, F.; Pierucci, D.; Silly, M.; Sirotti, F.; Rochet, F. Dissociation of Ethoxysilane and Methoxysilane on Si(001)-2 × 1 and Si(111)-7 × 7 at Room Temperature: A Comparative Study Using Synchrotron Radiation Photoemission. *J. Phys. Chem. C* **2014**, *118*, 24397–24406.

(49) Sun, D.; Huang, Y.; Han, B.; Yang, G. Ti-Si Mixed Oxides Prepared by Polymer In Situ Sol-Gel Chemistry with the Aid of CO₂. *Langmuir* **2006**, *22*, 4793–4798.

(50) Pabon, E.; Retuert, J.; Quijada, R.; Zarate, A. TiO₂–SiO₂ Mixed Oxides Prepared by a Combined Sol–gel and Polymer Inclusion Method. *Microporous Mesoporous Mater.* **2004**, *67*, 195–203.

(51) Methaapanon, R.; Bent, S. F. Comparative Study of Titanium Dioxide Atomic Layer Deposition on Silicon Dioxide and Hydrogen-Terminated Silicon. *J. Phys. Chem. C* **2010**, *114*, 10498–10504.

(52) Le, T. T. U.; Sasahara, A.; Tomitori, M. Water Wettability of an Ultrathin Layer of Silicon Oxide Epitaxially Grown on a Rutile Titanium Dioxide (110) Surface. *J. Phys. Chem. C* **2013**, *117*, 23621–23625.

(53) Gamble, L.; Jung, L. S.; Campbell, C. T. Decomposition and Protonation of Surface Ethoxys on TiO₂ (110). *Surf. Sci.* **1996**, *348*, 1–16.

(54) Idriss, H.; Kim, K. S.; Barteau, M. A. Carbon-Carbon Bond Formation via Aldolization of Acetaldehyde on Single Crystal and Polycrystalline TiO₂ Surfaces. *J. Catal.* **1993**, *139*, 119–133.

(55) Nadeem, A. M.; Muir, J. M. R.; Connelly, K. A.; Adamson, B. T.; Metson, B. J.; Idriss, H. Ethanol Photo-Oxidation on a Rutile TiO₂(110) Single Crystal Surface. *Phys. Chem. Chem. Phys.* **2011**, *13*, 7637–7643.

(56) Kim, Y. K.; Hwang, C.-C. Photoemission Study on the Adsorption of Ethanol on Clean and Oxidized Rutile TiO₂(110)-1 × 1 Surfaces. *Surf. Sci.* **2011**, *605*, 2082–2086.

(57) Benito, N.; Palacio, C. Mixed Ti-O-Si Oxide Films Formation by Oxidation of Titanium-Silicon Interface. *Appl. Surf. Sci.* **2014**, *301*, 436–441.